

Optimized numerical density functional theory calculation of rotationally symmetric jellium model systems

Guangdi Zhang(张广迪), Li Mao(毛力), and Hongxing Xu(徐红星)

Citation: Chin. Phys. B, 2024, 33 (**10**): 107101. DOI: 10.1088/1674-1056/ad655a
Journal homepage: http://cpb.iphy.ac.cn; http://iopscience.iop.org/cpb

What follows is a list of articles you may be interested in

Half-metallic ferromagnetic Weyl fermions related to dynamic correlations in the zinc-blende compound VAs

Xianyong Ding(丁献勇), Haoran Wei(魏皓然), Ruixiang Zhu(朱瑞翔), Xiaoliang Xiao(肖晓亮), Xiaozhi Wu(吴小志), and Rui Wang(王锐)
Chin. Phys. B, 2024, 33 (**9**): 097103. DOI: 10.1088/1674-1056/ad5f86

Coexistence of Dirac and Weyl points in non-centrosymmetric semimetal $NbIrTe_4$

Qingxin Liu(刘清馨), Yang Fu(付阳), Pengfei Ding(丁鹏飞), Huan Ma(马欢), Pengjie Guo(郭朋杰), Hechang Lei(雷和畅), and Shancai Wang(王善才)
Chin. Phys. B, 2024, 33 (**4**): 047104. DOI: 10.1088/1674-1056/ad2a79

Angle-resolved photoemission study of NbGeSb with non-symmorphic symmetry

Huan Ma(马欢), Ning Tan(谭宁), Xuchuan Wu(吴徐传), Man Li(李满), Yiyan Wang(王义炎), Hongyan Lu(路洪艳), Tianlong Xia(夏天龙), and Shancai Wang(王善才)
Chin. Phys. B, 2024, 33 (**2**): 027102. DOI: 10.1088/1674-1056/ad0ccf

Electronic structure of cuprate-nickelate infinite-layer heterostructure

Dachuan Chen(陈大川), Paul Worm, Liang Si(司良), Chunxiao Zhang(张春小), Fenglin Deng(邓凤麟), Peiheng Jiang(蒋沛恒), and Zhicheng Zhong(钟志诚)
Chin. Phys. B, 2023, 32 (**8**): 087105. DOI: 10.1088/1674-1056/acd368

Thermal spin molecular logic gates modulated by an electric field

Xingyi Tan(谭兴毅), Qiang Li(李强), and Dahua Ren(任达华)
Chin. Phys. B, 2023, 32 (**5**): 057101. DOI: 10.1088/1674-1056/ac89e5

Optimized numerical density functional theory calculation of rotationally symmetric jellium model systems

Guangdi Zhang(张广迪)[1], Li Mao(毛力)[1,2,†], and Hongxing Xu(徐红星)[1,2,3,4,‡]

[1] *School of Physics and Technology, Wuhan University, Wuhan* 430070, *China*
[2] *Wuhan Institute of Quantum Technology, Wuhan* 430205, *China*
[3] *School of Microelectronics, Wuhan University, Wuhan* 430072, *China*
[4] *Henan Academy of Sciences, Zhengzhou* 450046, *China*

(Received 21 May 2024; revised manuscript received 11 July 2024; accepted manuscript online 19 July 2024)

In real space density functional theory calculations, the effective potential depends on the electron density, requiring self-consistent iterations, and numerous integrals at each step, making the process time-consuming. In our research, we propose an optimization method to expedite density functional theory (DFT) calculations for systems with large aspect ratios, such as metallic nanorods, nanowires, or scanning tunneling microscope tips. This method focuses on employing basis set to expand the electron density, Coulomb potential, and exchange–correlation potential. By precomputing integrals and caching redundant results, this expansion streamlines the integration process, significantly accelerating DFT computations. As a case study, we have applied this optimization to metallic nanorod systems of various radii and lengths, obtaining corresponding ground-state electron densities and potentials.

Keywords: density functional theory, basis set, integrals precomputation, nanorod

PACS: 71.15.Mb, 02.60.Pn, 81.16.–c **DOI:** 10.1088/1674-1056/ad655a

1. Introduction

Density functional theory (DFT)[1–6] is an essential methodology and a powerful tool for studying multi-electron systems which offers rich information about electron clouds. It has proven successful in determining the electronic structure of atoms, molecules, and solids, and has wide applications in various fields such as physics, chemistry and biology. The success of this theory has been facilitated by the rapid increase in computational power[7–11] in recent years, making high-precision simulations of complex systems feasible. It has been extensively applied in simulating diverse systems ranging from small molecules to large biological macromolecules and solid-state materials. It has emerged as a "standard tool"[12] in the realm of quantum computing. Since its inception, DFT has stood as the foremost and indispensable technology in condensed matter physics, enabling the calculation of electronic structures and their properties.

Surface plasmons are a type of elementary excitation formed by strong coupling between electromagnetic fields and collective oscillations of free electrons in solids,[13–15] which can localize the light field within the subwavelength range that breaks the diffraction limit. For example, the nano gaps between metal particles[16–18] are referred to as "hotspots".[19] The electric field intensity is enhanced by plasmon resonance, and the enhancement factor can even reach 10^2, resulting in a significant enhancement of the molecular Raman scattering signal inside the gap (as the Raman signal is proportional to the 4th power of the electric field, the maximum can reach 10^8), which is surface enhanced Raman spectroscopy (SERS).[20,21] Generally speaking, the smaller the gap spacing, the greater the electric field enhancement. However, when the gap is small to the nanoscale, quantum effects will take effect.[22–25] Previously, only classical electromagnetic methods were used to calculate the electromagnetic field, which would fail.[26–28] At this point, DFT calculations can be used[29–31] in order to include the quantum effect and obtain more accurate results. By calculating the electronic structure and dielectric function of metal surfaces, DFT can accurately describe the resonance frequency and intensity of plasmons. DFT is also used to study the adsorption behavior of molecules on metal surfaces, helping to reveal the chemical enhancement mechanisms of SERS and other phenomena. This makes DFT a key tool for designing and optimizing plasmon materials and devices. Also, DFT can be applied to the relevant calculations of scanning tunneling microscope (STM) systems. STM relies on the tunnel current between the metal tip and the sample surface, which is very sensitive to the electronic structure of the area near the metal tip to the sample.[32] The DFT can be used to calculate such areas with high accuracy, which helps to understand STM images and spectral data. For example, STM studies have shown that MoS_2 clusters below 2 nm–3 nm may exhibit new structural and electronic properties, and this can be verified by DFT.[33]

The key to DFT lies in the rapid and accurate solution of

†Corresponding author. E-mail: maoli@whu.edu.cn
‡Corresponding author. E-mail: hxxu@whu.edu.cn

© 2024 Chinese Physical Society and IOP Publishing Ltd

the Kohn–Sham equation.[34,35] However, in practical applications, many systems have very large scales, even reaching the micrometer level. Taking a gold nanorod with diameter of 10 nm and length of 1 μm as an example, the number of electrons can reach the million level. To achieve sufficiently accurate computational results, it is necessary to expand the wave functions with a large number of basis functions. Consequently, the matrix dimension of the Hamiltonian in the Kohn–Sham equation becomes extremely large. When the matrix dimension becomes too large, computational demands increase significantly (the computational complexity of diagonalizing the matrix is $O(N^3)$, and potential integrals of the order of N^2 need to be computed). This places considerable pressure on computational resources and may even render calculations infeasible due to the extremely large matrix dimensions. If one were to directly reduce the number of basis functions to expedite computation, it would result in significant errors in the computational results. Hence, there is an urgent need for new algorithms to accelerate large-scale density functional theory calculations.

Due to the complexity of DFT calculations, researchers have been exploring optimization methods from various perspectives to solve the problem of high computational complexity and long computational time in DFT. Here are some existing methods. For example, parallel computing can be utilized to accelerate computation through high-performance computing clusters.[36–38] Also, quantum mechanics and classical electromagnetic methods can also be mixed together. Divide the system into quantum intervals and classical intervals as needed, solve it using time-domain Maxwell equations in the classical interval, and solve it using DFT and Green's function in the quantum mechanics interval.[39,40] In addition, various approximation methods, such as density functional tight binding (DFTB)[41–46] and semiempirical methods,[47–49] can also optimize computational speed. And although directly reducing the number of system basis functions can reduce the accuracy of calculations, it is possible to strike a balance between accuracy and computational cost, and to accelerate calculations by cleverly selecting and constructing basis set without affecting accuracy as much as possible. For example, there is an article[50] that constructes a composite basis set of plane waves and Gaussian or spline functions, and compares it with strict computational methods, it has been verified that the composite matrix group can ensure solution accuracy while accelerating calculations. Finally, machine learning methods[51–56] can also be used to accelerate the calculation of DFT.

The calculation of DFT can be done in real space or momentum space. Usually, the momentum space DFT is more suitable for periodic systems and small systems, while the real space DFT is more suitable for large systems. Various softwares have different choices, for instance, VASP[57] is a DFT method in momentum space that utilizes pseudopotential and plane wave basis set. Octopus[58] uses the real space grid method. And Gaussian[59] expands the wave function with Gaussian basis set. We adopted the real space DFT. In this calculations, it is necessary to use the Kohn–Sham equation to compute the electron density, the Coulomb potential, and the exchange–correlation potential through a self-consistent iteration process. However, in each step of this self-consistent calculation, a substantial number of integrals need to be computed[60] to get the Hamiltonian matrix elements of the effective potential, and integral calculations can often be quite time-consuming for large systems. Furthermore, a significant amount of redundant calculations arises during the computational process, as some integrals or matrix elements remain constant or change only slightly between iterations.

In this paper, we develope an optimization method, the electron density, Coulomb potential, and exchange–correlation potential in the Kohn–Sham equation are all expanded by a set of basis functions. By doing so, we can simplify integrals in advance during the computational process and store some of the repetitive calculation results. This not only eliminates the need for recalculating integrals within the self-consistent loop but also reduces a significant amount of redundant computations. In this method, Coulomb potential does not require integration calculations anymore, and the integration calculations of exchange–correlation potential is also significantly simplified. Leveraging this optimization can notably accelerate the computational speed of DFT calculations. This optimization utilizes the product of Bessel functions, so it is more effective for rotational symmetry systems. This article uses the jellium model, also known as the homogeneous electron gas model, which is different from the all electronic model or pseudopotentials method. We have implemented the aforementioned computation in our program and validated it on a system of metal nanorods. The results of our calculations demonstrate that our method not only enhances computational speed but also accurately computes jellium model systems with rotational symmetry (note that this method can also be applied in systems without rotational symmetry).

2. Computational methods

For systems with a large aspect ratio, such as nanorods, nanowires, or STM tips, it is more convenient to apply the Kohn–Sham (KS) Hamiltonian in cylindrical coordinates

$$\hat{H}_{\mathrm{KS}} = -\frac{\hbar^2}{2m_{\mathrm{e}}}\nabla^2 + V_{\mathrm{xc}}(x,r,\theta) + V_{\mathrm{c}}(x,r,\theta), \tag{1}$$

where V_{xc} is the exchange–correlation potential, it can be expressed as a function of electron density $\rho_{\mathrm{e}}(x,r,\theta)$ or the local Wigner–Seitz radius $r_{\mathrm{s}}(x,r,\theta)$. V_{c} is the Coulomb potential. The cylindrical coordinate system is particularly suitable for

systems with rotational symmetry and can significantly simplify the calculation process of integration, especially when the integration region has cylindrical symmetry. The eigen functions of KS Hamiltonian $\Psi_{mj}(x,r,\theta)$ (surppose our system has rotational symmetry, and m is a good quantum number, j means the j-th eigen-function of angular quantum number m) can be expanded as $\Psi_{mj}(x,r,\theta)=\sum_n\sum_{l=1}^{L_{\rm cut}}a^j_{mnl}|mnl\rangle$, with the basis

$$\begin{aligned}
&|mnl\rangle=\omega_m(\theta)j_{mn}(r)s_l(x),\quad \omega_m(\theta)=\frac{1}{\sqrt{2\pi}}\mathrm{e}^{\mathrm{i}m\theta},\\
&j_{mn}(r)=\frac{\sqrt{2}}{\mathrm{J}_{m+1}(Q_{mn})R}\mathrm{J}_m\left(\frac{Q_{mn}}{R}r\right),\\
&s_l(x)=\sqrt{\frac{2}{L}}\sin\left(\frac{l\pi}{L}x\right)=-\mathrm{i}[c_l(x)-c_{-l}(x)],
\end{aligned}\tag{2}$$

where $\omega_m(\theta)$, $j_{mn}(r)$, and $s_l(x)$ are the eigen-functions in each coordinate of θ, r, and x. And J_m is the m-th Bessel function, Q_{mn} is its n-th zero point, and $c_l(x)=\sqrt{1/2L}\exp(\mathrm{i}\pi x/L)$. Note that ω_m and j_{mn} can be used to expand any functions. But $s_l(x)$ can only be applied to wave functions which satisfy boundary conditions. In order to expand Coulomb potential and electron number density, one can extend the domain of x from $[0,L]$ to $[0,2L]$, and use $c_l(x)$ instead. Also, we need to extend the summation section of l from $[1,L_{\rm cut}]$ to $[-L_{\max},L_{\max}]$. For example, if we have a function $f(x,r,\theta)$, it can be expanded as

$$f(x,r,\theta)=\sum_{l=-L_{\max}}^{L_{\max}}\sum_{mn}f_{mnl}c_l(x)j_{mn}(r)\omega_m(\theta).\tag{3}$$

Here f_{mnl} are expansion coefficients, if $f(x,r,\theta)$ is a real function, the real parts of f_{mnl} are symmetric under transformation $l\to -l$, while the imaginary parts are anti-symmetric ($\mathrm{Re}[f_{mnl}]=\mathrm{Re}[f_{mn(-l)}]$, $\mathrm{Im}[f_{mnl}]=-\mathrm{Im}[f_{mn(-l)}]$). Because m is a good quantum number and both the exchange–correlation potenial energy $V_{\rm xc}(x,r,\theta)$ and Coulomb potenial energy $V_{\rm c}(x,r,\theta)$ are real functions, one can find the Hamiltonian matrix elements $H_{mn_1l_1n_2l_2}=\langle mn_1l_1|\hat{H}|mn_2l_2\rangle$ and the wave function expansion coefficients a^j_{mnl} are both real.

2.1. Expanding electron density

The electron density $\rho_{\rm e}=2\sum_{mj}|\Psi_{mj}|^2$ (2 for spin degeneracy) can be expanded by Eq. (3)

$$\rho_{\rm e}(x,r,\theta)=\sum_{l=-L_{\max}}^{L_{\max}}\sum_{mn}d_{mnl}c_l(x)j_{mn}(r)\omega_m(\theta).\tag{4}$$

Keep in mind that the summation of l here (from $-L_{\max}$ to $L_{\max}$) is a little different to the summation in wave function (from 1 to $L_{\rm cut}$), and we will ignore the notaion from now on. Because our system has rotaional symmetry, so the electron density does not depend on θ, and for $m\neq 0$ we have $d_{mnl}=0$. In order to simplify the notation, we use d_{nl} instead from now on. By setting $\rho_{\rm e}=0$ in section $[L,2L]$, one can get

$$\begin{aligned}
d_{nl}=&-\frac{1}{2}\sqrt{\frac{1}{L\pi}}\sum_{mjn_1n_2l_1l_2}a^j_{mn_1l_1}a^j_{mn_2l_2}\mathrm{I}_{mn_1n_2n}\int_0^1[\mathrm{e}^{\mathrm{i}(l_{\rm p}-l)\pi x}\\
&+\mathrm{e}^{\mathrm{i}(-l_{\rm p}-l)\pi x}-\mathrm{e}^{\mathrm{i}(l_{\rm m}-l)\pi x}-\mathrm{e}^{\mathrm{i}(-l_{\rm m}-l)\pi x}]\mathrm{d}x,
\end{aligned}\tag{5}$$

where $l_{\rm p,m}=l_1\pm l_2$, and we have defined triplet Bessel function integrations, $\mathrm{I}_{mn_1n_2n}$, which can be calculated and stored before the main program to accelerate computing. The calculation of integrals is the most time-consuming throughout the entire calculation process. We store triple Bessel function integrations in advance which can avoid a large amount of redundant calculations.

$$\mathrm{I}_{mn_1n_2n}=\int_0^R j_{mn_1}(r)j_{mn_2}(r)j_{0n}(r)r\mathrm{d}r.\tag{6}$$

For more details, please see Appendix A.

For matrix elements, originally we need to calculate the integrals of the product of three Bessel functions for $N_{\rm w}^2$ instances (actual calculations are more complex), in our program it can be transformed into the integrals of the product of three Bessel functions for $N_{\rm d}$ instances and multiplication calculations for $N_{\rm d}\times N_{\rm w}^2$ instances. $N_{\rm w}$ is the total number of basis functions for wave functions, and $N_{\rm d}$ is the total number of basis functions for electron density and potentials. After testing, it was found that using single core of Intel Xeon E5-2650 v2 CPU, one calculation of the integral takes about 0.95 ms, and one calculation of multiplication takes about 6.3×10^{-6} ms. The value of $N_{\rm d}$ is approximately 10^4, and is much smaller than $N_{\rm w}^2$. This means that in the most time-consuming part of our calculation, which is the calculation of matrix elements, approximately an order of magnitude of time can be saved.

2.2. Expanding Coulomb and exchange–correlation potentials

Also, the Coulomb potential $V_{\rm c}(x,r,\theta)$ and exchange–correlation potential $V_{\rm xc}(x,r,\theta)$ can be expanded as

$$V_{\rm c,xc}(x,r,\theta)=\sum_{mnl}v^{\rm c,xc}_{mnl}c_l(x)j_{mn}(r)\omega_m(\theta).\tag{7}$$

Note that for Coulomb potential we have the Poisson's equation

$$\nabla^2V_{\rm c}(x,r,\theta)=4\pi[\rho_{\rm p}(x,r)-\rho_{\rm e}(x,r,\theta)],\tag{8}$$

where we have used the atomic units (a.u). $\rho_{\rm p}(x,r)$ is the backgroud charge density

$$\rho_{\rm p}(x,r)=\begin{cases}\rho_{\rm p}^0, & x\in[x_0,x_0+L],r\in[0,R],\\ 0, & \text{otherwise.}\end{cases}\tag{9}$$

Because of the same reason for density expansion coefficients, $v^{\rm c,xc}_{mnl}$ should not be dependent on m, so one can use $v^{\rm c,xc}_{nl}$ instead. Now

$$\nabla^2V_{\rm c}(x,r,\theta)=-\sqrt{\frac{1}{2\pi}}\sum_{nl}\left(\frac{Q_{0n}^2}{R^2}+\frac{l^2}{L^2}\pi^2\right)v^{\rm c}_{nl}c_l(x)j_{0n}(r),\tag{10}$$

and the expansion coefficients for Coulomb potential read

$$v_{nl}^{\mathrm{c}} = \frac{4\pi}{Q_{0n}^2/R^2 + l^2\pi^2/L^2}\sqrt{\frac{1}{2\pi}}\int c_l^*(x) j_{0n}(r)[\rho_{\mathrm{e}}(x,r,\theta) - \rho_{\mathrm{p}}(x,r)] r\,\mathrm{d}r\,\mathrm{d}\theta\,\mathrm{d}x, \tag{11}$$

which contains two parts $v_{nl}^{\mathrm{c}} = v_{nl}^{\mathrm{cp}} + v_{nl}^{\mathrm{ce}}$, the first part can be directly integrated,

$$v_{nl}^{\mathrm{cp}} = -\frac{2(2\pi)^{3/2}}{Q_{0n}^2/R^2 + l^2\pi^2/L^2}\rho_{\mathrm{p}}^0 \times \int_{x_0}^{x_0+L_0} c_l^*(x)\,\mathrm{d}x \int_0^{R_0} j_{0n}(r) r\,\mathrm{d}r. \tag{12}$$

Here x_0, x_0+L_0, R_0 are the rod boundaries where the inside positive charge density ρ_{p} goes to zero. For the second part, one can find

$$v_{nl}^{\mathrm{ce}} = \frac{4\pi}{Q_{0n}^2/R^2 + l^2\pi^2/L^2} d_{nl}. \tag{13}$$

In DFT calculations, under the LDA approximation, one commonly used form (when Wigner–Seitz radius $r_{\mathrm{s}} \geq 1$) for exchange–correlation potential V_{xc} is the exact uniform solution[1,2,61] obtained through the Monte Carlo method

$$\begin{aligned} E_{\mathrm{xc}}(\rho_{\mathrm{e}}) &= \int \rho_{\mathrm{e}}(\boldsymbol{r})\varepsilon_{\mathrm{xc}}(\rho_{\mathrm{e}}(\boldsymbol{r}))\,\mathrm{d}\boldsymbol{r}, \\ \varepsilon_{\mathrm{xc}} &= \varepsilon_{\mathrm{x}} + \varepsilon_{\mathrm{c}}, \\ \varepsilon_{\mathrm{x}} &= -0.916/r_{\mathrm{s}}, \\ \varepsilon_{\mathrm{c}} &= -0.2846/(1 + 1.0529\sqrt{r_{\mathrm{s}}} + 0.3334), \\ V_{\mathrm{xc}} &= \frac{\delta E_{\mathrm{xc}}(\rho_{\mathrm{e}})}{\delta\rho_{\mathrm{e}}} = \varepsilon_{\mathrm{xc}}(\rho_{\mathrm{e}}) + \rho_{\mathrm{e}}\frac{\partial\varepsilon_{\mathrm{xc}}(\rho_{\mathrm{e}})}{\partial\rho_{\mathrm{e}}}, \end{aligned} \tag{14}$$

where ε_{x} is exchange energy, ε_{c} is correlation energy, $\varepsilon_{\mathrm{xc}}$ is exchange–correlation energy, and E_{xc} is exchange–correlation functional. After expanding V_{xc} with Eq. (3) by numerical method as Eq. (14), we have all the components needed to calculating the Hamiltonian's matrix elements, and get

$$H_{mn_1l_1n_2l_2} = \frac{1}{2}\left(\frac{Q_{mn_1}^2}{R^2} + \frac{l_1^2}{L^2}\pi^2\right)\delta_{n_1n_2}\delta_{l_1l_2} + \mathcal{V}_{mn_1n_2l_1l_2}^{\mathrm{xc}} + \mathcal{V}_{mn_1n_2l_1l_2}^{\mathrm{c}}. \tag{15}$$

The detail expressions for exchange–correlation and Coulomb terms $\mathcal{V}_{mn_1n_2l_1l_2}^{\mathrm{xc,c}}$ can be found in Appendix B. Where one can find we do not need to calculate integrations for Coulomb terms and reduce N_{w}^2 integrations to N_{d} integrations for exchange–correlation terms.

3. Examples and discussion

In order to validate the optimization process presented in this paper, we utilize the principles of DFT in conjunction with the optimization method to compute the ground-state properties of silver nanorods. These properties encompass energy level distribution, electron density distribution, Coulomb potential, exchange–correlation potential, and more. We have implemented the above calculations using C++ and Python, then we perform an analysis and validation of the computational results. Further calculations can also be conducted to explore additional properties, such as the electron tunneling phenomena.

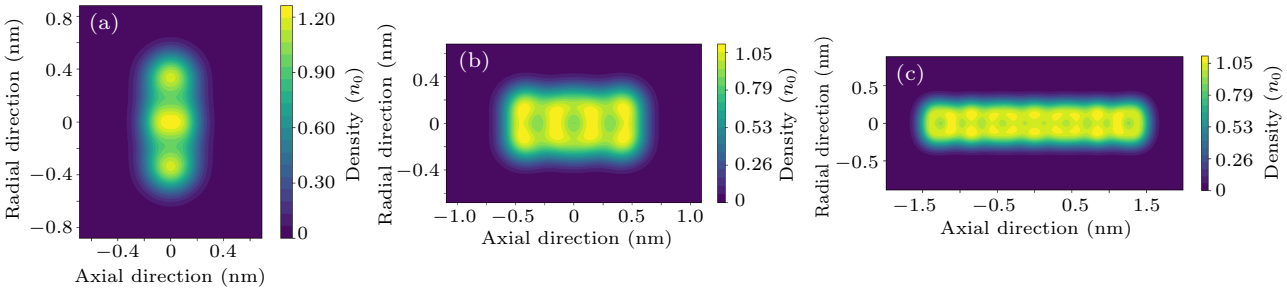


Fig. 1. The calculated electron density distribution of silver nanorod. n_0 is the average electron density. Each subgraph represents nanorods of different sizes, panel (a) has a diameter of 1 nm and a length of 0.4 nm, panel (b) has a diameter of 0.6 nm and a length of 1.2 nm, and panel (c) has a diameter of 0.6 nm and a length of 3 nm.

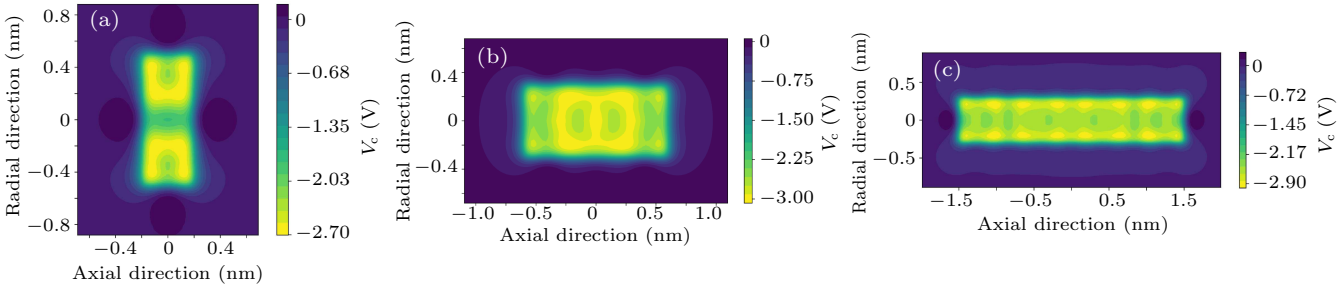


Fig. 2. The calculated Coulomb potential distribution of silver nanorod. Each subgraph represents nanorods of different sizes, panel (a) has a diameter of 1 nm and a length of 0.4 nm, panel (b) has a diameter of 0.6 nm and a length of 1.2 nm, and panel (c) has a diameter of 0.6 nm and a length of 3 nm.

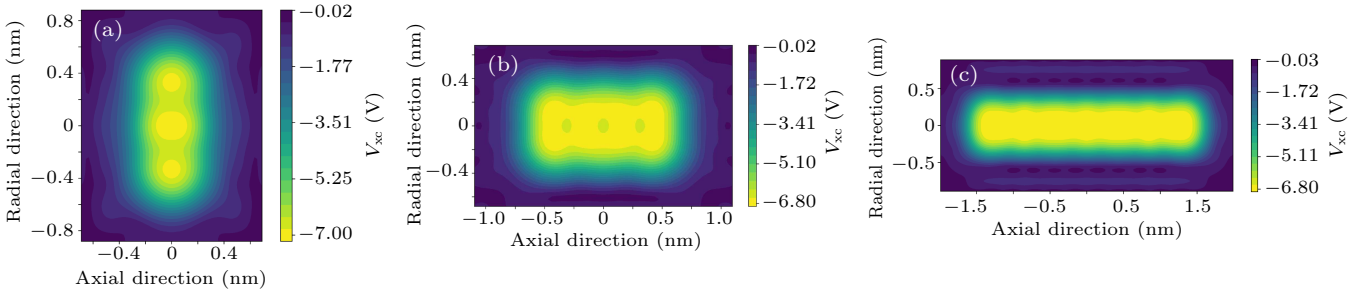


Fig. 3. The calculated exchange–correlation potential distribution of silver nanorod. Each subgraph represents nanorods of different sizes, panel (a) has a diameter of 1 nm and a length of 0.4 nm, panel (b) has a diameter of 0.6 nm and a length of 1.2 nm, and panel (c) has a diameter of 0.6 nm and a length of 3 nm.

Our method and program can calculate nanorods of different sizes and column length to diameter ratios. Here we calculated silver nanorods of three different sizes. Once the iterative computations of the Kohn–Sham equation have converged to stable results, we observe the electron density distributions, Coulomb potential distributions, and exchange–correlation potential distributions of this systems, as depicted in Figs. 1–3. Generally, each calculation requires over a hundred iterations.

In these figures, firstly it is evident that these distributions align with the dimensions of the nanorod. Secondly, it can be seen that these distributions are symmetric about the center of the nanorod. Thirdly, it can be seen that our results conform to basic physical laws. For electron density distribution in Fig. 1, generally speaking, the closer to the center of the nanorod, the higher the electron density. At the edge of the nanorod, the electron density rapidly decreases and eventually becomes zero. The distribution of Coulomb potential or exchange–correlation potential also follows a similar pattern. For nanorods of different sizes, the maximum calculated Coulomb potential and exchange–correlation potential are very close under the same initial conditions. And in these figures, it can be seen that the results have obvious periodicity. Electron density, Coulomb potential, and exchange–correlation potential all oscillate periodically around the average value, with a period of $\lambda_f/2$. λ_f is the Fermi wavelength of silver. From these figures, it can be estimated that the Fermi wavelength is approximately 0.5 nm–0.6 nm, and the theoretical value of the Fermi wavelength for the bulk sliver we use is 0.52 nm. These two values are relatively close, and the larger the size, the closer the calculated value is to the theoretical value.

We can see that for nanorods of different sizes, the depths of the effective potential (i.e., the sum of Coulomb potential and exchange–correlation potential) well oscillate slightly with the size of nanorods. And in our calculations, the work function of silver nanorods is approximately 3 eV–4 eV for different sizes, which is very close to those obtained through jellium model in other articles.[62,63] This results further demonstrates that our calculation is correct.

Except silver nanorods, our method can also calculate other metals, such as Au, Al, and Pt. As an example, we present the calculation results of gold nanorod in Fig. 4.

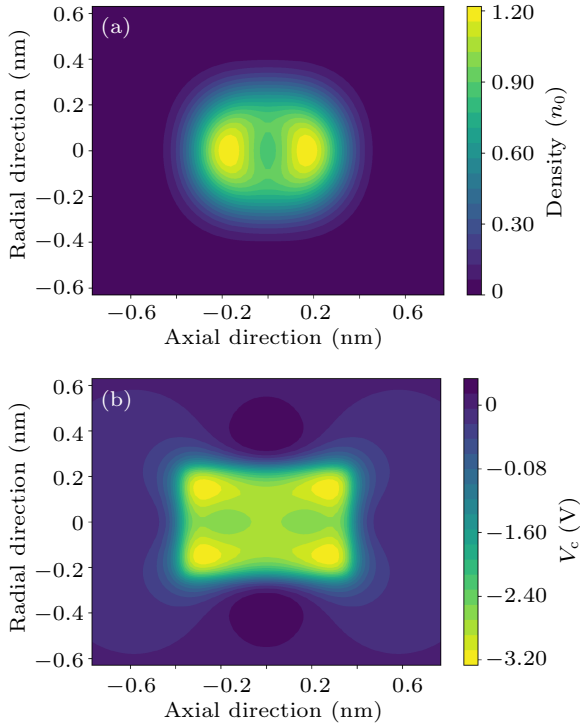


Fig. 4. The calculated distribution of gold nanorod with a diameter of 0.48 nm and a length of 0.75 nm. Panel (a) is the electron density distribution, and panel (b) is the Coulomb potential distribution.

4. Conclusion

We introduce an effective optimization method to accelerate DFT calculations by using a basis set, which is analytically extended from the basis set for wave functions, to expand the electron density, Coulomb potential, and exchange–correlation potential. In this method, Coulomb potential no longer requires integration calculations, while the number of integrations associated with the exchange–correlation potential has been reduced from N_w^2 (N_w is the total number of basis functions for expanding wave functions) to N_d (the total number of basis functions for expanding electron density and potentials). Through this method, we have successfully reduced redundant calculations and accelerated computation speed. The validation of the metal nanorod system confirms the effectiveness and accuracy of our method. This optimiza-

tion strategy is expected to improve the efficiency and scalability of DFT calculations in various applications.

Appendix A: Density expansion

The electron density

$$\rho_{\rm e} = 2\sum_{mj}|\Psi_{mj}|^2 = \sum_{mn_1l_1n_2l_2} a_{mn_1l_1}a_{mn_2l_2}j_{mn_1}(r)j_{mn_2}(r) \times [c_{l_{\rm m}}(x)+c_{-l_{\rm m}}(x)-c_{l_{\rm p}}(x)-c_{-l_{\rm p}}(x)], \tag{A1}$$

where $l_{\rm p,m} = l_1 \pm l_2$. $\rho_{\rm e}$ can be expanded with Eq. (3), one can find

$$d_{nl} = \frac{1}{2}\sqrt{\frac{1}{L\pi}}\sum_{mn_1n_2}{\rm I}_{mn_1n_2n}A_{mn_1n_2l}, \tag{A2}$$

$${\rm I}_{mn_1n_2n} = \int_0^R j_{mn_1}(r)j_{mn_2}(r)j_{0n}(r)r\,{\rm d}r, \tag{A3}$$

$$A_{mn_1n_2l} = \sum_{jl_1l_2} a^j_{mn_1l_1}a^j_{mn_2l_2}\int_0^1[{\rm e}^{{\rm i}(l_{\rm m}-l)\pi x}+{\rm e}^{{\rm i}(-l_{\rm m}-l)\pi x} - {\rm e}^{{\rm i}(l_{\rm p}-l)\pi x}-{\rm e}^{{\rm i}(-l_{\rm p}-l)\pi x}]\,{\rm d}x. \tag{A3}$$

The real part of $A_{mn_1n_2l}$ reads

$${\rm Re}[A_{mn_1n_2l}] = \sum_{jl_1l_2} a^j_{mn_1l_1}a^j_{mn_2l_2} \times(\delta_{l+l_{\rm m}}+\delta_{l-l_{\rm m}}-\delta_{l+l_{\rm p}}-\delta_{l-l_{\rm p}}). \tag{A5}$$

The image part of $A_{mn_1n_2l}$ reads

$${\rm Im}[A_{mn_1n_2l}] = \frac{4l}{\pi}\sum_{jl_1l_2}\frac{(l_{\rm p}^2-l_{\rm m}^2)P_{l+l_{\rm p}}}{(l_{\rm p}^2-l^2)(l_{\rm m}^2-l^2)}a^j_{mn_1l_1}a^j_{mn_2l_2}, \tag{A6}$$

where P_l is the parity of integer l

$$P_l = \begin{cases} 1, & l \text{ is odd}, \\ 0, & l \text{ is even}. \end{cases} \tag{A6}$$

Obviously, the real parts of density expansion coefficients are symmetric under the transformation $l \to -l$ while the imaginary parts are anti-symmetric.

Appendix B: Hamiltonian matrix elements of exchange–correlation and Coulomb potentials

The Coulomb potenial can be expanded with Eq. (7), and one can get the expanding coefficients with Eqs. (11)–(13). About the exchange–correlation potential, we need to calculate $N_{\rm d}$ numerical integrations ($N_{\rm d}$ is the total number of basis funcitons for expanding electron density and potenials). Once we get the coefficients, their Hamiltonian elements read

$$\mathcal{V}^{\rm xc,c}_{m,n_1n_2l_1l_2} = \langle mn_1l_1|V_{\rm xc,c}(x,r,\theta)|mn_1l_1\rangle = \frac{1}{4}\sqrt{\frac{1}{L\pi}}\sum_n {\rm I}_{mn_1n_2n}B^{\rm xc,c}_{nl_1l_2}, \tag{B1}$$

where

$$B^{\rm xc,c}_{nl_1l_2} = \sum_{l=-L_{\rm max}}^{L_{\rm max}} v^{\rm xc,c}_{nl}\int_0^1[{\rm e}^{{\rm i}(l_{\rm m}-l)\pi x}+{\rm e}^{{\rm i}(-l_{\rm m}-l)\pi x} - {\rm e}^{{\rm i}(l_{\rm p}-l)\pi x}-{\rm e}^{{\rm i}(-l_{\rm p}-l)\pi x}]\,{\rm d}x = \sum_{l=0}^{L_{\rm max}}[2-\delta(l)]\{[\delta(l+l_{\rm m})+\delta(l-l_{\rm m}) - \delta(l+l_{\rm p})-\delta(l-l_{\rm p})]\,{\rm Re}[v^{\rm xc,c}_{nl}] + \frac{4l}{\pi}\frac{(l_{\rm p}^2-l_{\rm m}^2)P_{l+l_{\rm p}}}{(l_{\rm p}^2-l^2)(l_{\rm m}^2-l^2)}\,{\rm Im}[v^{\rm xc,c}_{nl}]\}. \tag{B2}$$

Acknowledgements

Project supported by the National Key Research and Development Program of China (Grant No. 2020YFA0211303) and the National Natural Science Foundation of China (Grant No. 91850207). And the numerical calculations in this paper have been done on the supercomputing system in the Supercomputing Center of Wuhan University.

References

[1] Engel E 2011 *Density functional theory* (Berlin: Springer) pp. 109–169
[2] Li Z Z 2002 *Solid State Theory* (Beijing: Higher Education Press) pp. 329–341 (in Chinese)
[3] Burke K 2012 *J. Chem. Phys.* **136** 150901
[4] Argaman N and Makov G 2000 *Am. J. Phys.* **68** 69
[5] Runge E and Gross E K 1984 *Phys. Rev. Lett.* **52** 997
[6] Marques M A and Gross E K 2004 *Annu. Rev. Phys. Chem.* **55** 427
[7] Jia W L, Cao Z Y, Wang L, Fu J Y, Chi X B, Gao W G and Wang L W 2013 *Comput. Phys. Commun.* **184** 9
[8] Jia W L, Fu J Y, Cao Z Y, Wang L, Chi X B, Gao W G and Wang L W 2013 *J. Comput. Phys.* **251** 102
[9] Nitsche M A, Ferreria M, Mocskos E E and Gonzalez Lebrero M C 2014 *J. Chem. Theory Comput.* **10** 959
[10] Ratcliff L E, Degomme A, Flores-Livas J A, Goedecker S and Genovese L 2018 *J. Phys.: Condens. Matter* **30** 095901
[11] Das S, Motamarri P, Subramanian V, Rogers D M and Gavini V 2022 *Comput. Phys. Commun.* **280** 108473
[12] Politzer P and Seminario J M 1995 *Modern density functional theory: a tool for chemistry* (Amsterdam: Elsevier) pp. 3-11
[13] Ghosh S K and Pal T 2007 *Chem. Rev.* **107** 4797
[14] Romero I, Aizpurua J, Bryant G W and De Abajo F J G 2006 *Opt. Express* **14** 9988
[15] Schuller J A, Barnard E S, Cai W, Jun Y C, White J S and Brongersma M L 2010 *Nat. Mater.* **9** 193
[16] Baumberg J J, Aizpurua J, Mikkelsen M H and Smith D R 2019 *Nat. Mater.* **18** 668
[17] Benz F, Schmidt M K, Dreismann A, Chikkaraddy R, Zhang Y, Demetriadou A, Carnegie C, Ohadi H, De Nijs B, Esteban R, Aizpurua J and Baumberg J J 2016 *Science* **354** 726
[18] Hao E and Schatz G C 2004 *J. Chem. Phys.* **120** 357
[19] Xu H X, Bjerneld E J, Kll M and Brjesson L 1999 *Phys. Rev. Lett.* **83** 4357
[20] Michaels A M, Jiang J and Brus L 2000 *J. Phys. Chem. B* **104** 11965
[21] Chen H J, Shao L, Li Q and Wang J F 2013 *Chem. Soc. Rev.* **42** 2679
[22] Pines D 1953 *Phys. Rev.* **92** 626
[23] Hopfield J 1958 *Phys. Rev.* **112** 1555
[24] Elson J and Ritchie R 1971 *Phys. Rev. B* **4** 4129
[25] Waks E and Sridharan D 2010 *Phys. Rev. A* **82** 043845
[26] Li Z P and Xu H X 2007 *J. Quant. Spectrosc. Radiat. Transfer* **103** 394
[27] Flatau P J, Fuller K A and Mackowski D W 1993 *Appl. Opt.* **32** 3302
[28] Futamata M, Maruyama Y and Ishikawa M 2003 *J. Phys. Chem. B* **107** 7607
[29] Mao L, Li Z P, Wu B and Xu H X 2009 *Appl. Phys. Lett.* **94** 243102
[30] Zuloaga J, Prodan E and Nordlander P 2009 *Nano Lett.* **9** 887
[31] Suo P F, Mao L, Shi J and Xu H X 2022 *Nanomaterials* **12** 1746

[32] Magonov S N and Whangbo M H 2008 *Surface analysis with STM and AFM: experimental and theoretical aspects of image analysis* (New York: John Wiley & Sons) pp. 1–56

[33] Besenbacher F, Brorson M, Clausen B S, Helveg S, Hinnemann B, Kibsgaard J, Lauritsen J V, Moses P G, Nrskov J K and Topse H 2008 *Catal. Today* **130** 86

[34] Kohn W and Sham L J 1965 *Phys. Rev.* **140** A1133

[35] Perdew J P, Ruzsinszky A, Tao J, Staroverov V N, Scuseria G E and Csonka G I 2005 *J. Chem. Phys.* **123** 062201

[36] Neese F, Wennmohs F, Hansen A and Becker U 2009 *Chem. Phys.* **356** 98

[37] Hu W, Lin L and Yang C 2015 *J. Chem. Phys.* **143** 124110

[38] Shimojo F, Kalia R K, Nakano A and Vashishta P 2001 *Comput. Phys. Commun.* **140** 303

[39] Meng L, Yam C, Koo S, Chen Q, Wong N and Chen G 2012 *J. Chem. Theory Comput.* **8** 1190

[40] Yam C, Meng L, Chen G, Chen Q and Wong N 2011 *Phys. Chem. Chem. Phys.* **13** 14365

[41] Elstner M, Porezag D, Jungnickel G, Elsner J, Haugk M, Frauenheim T, Suhai S and Seifert G 1998 *Phys. Rev. B* **58** 7260

[42] Elstner M and Seifert G 2014 *Philos. Trans. R. Soc. A* **372** 20120483

[43] Koskinen P and Mkinen V 2009 *Comput. Mater. Sci.* **47** 237

[44] Spiegelman F, Tarrat N, Cuny J, Dontot L, Posenitskiy E, Mart C, Simon A and Rapacioli M 2020 *Adv. Phys. X* **5** 1710252

[45] Liu T X, Mao L, Pistol M E and Pryor C 2022 *J. Phys.: Condens. Matter* **34** 125901

[46] Liu T X, Pistol M E, Pryor C and Mao L 2022 *Comput. Mater. Sci.* **211** 111479

[47] Cui Q and Elstner M 2014 *Phys. Chem. Chem. Phys.* **16** 14368

[48] Thiel W 2014 *Wires. Comput. Mol. Sci.* **4** 145

[49] Mehta N, Casanova-Pez M and Goerigk L 2018 *Phys. Chem. Chem. Phys.* **20** 23175

[50] Zhang G D, Mao L and Xu H X 2023 *Acta Phys. Sin.* **72** 180302 (in Chinese)

[51] Schleder G R, Padilha A C, Acosta C M, Costa M and Fazzio A 2019 *J. Phys. Mater.* **2** 032001

[52] Jinnouchi R and Asahi R 2017 *J. Phys. Chem. Lett.* **8** 4279

[53] Ulissi Z W, Medford A J, Bligaard T and Nrskov J K 2017 *Nat. Commun.* **8** 14621

[54] Faber F A, Hutchison L, Huang B, Gilmer J, Schoenholz S S, Dahl G E, Vinyals O, Kearnes S, Riley P F and Von Lilienfeld O A 2017 *J. Chem. Theory Comput.* **13** 5255

[55] Dragoni D, Daff T D, Csnyi G and Marzari N 2018 *Phys. Rev. Mater.* **2** 013808

[56] Wei J, Chu X, Sun X Y, Xu K, Deng H X, Chen J G, Wei Z M and Lei M 2019 *InfoMat* **1** 338

[57] Hafner J 2008 *J. Comput. Chem.* **29** 2044

[58] Marques M A, Castro A, Bertsch G F and Rubio A 2003 *Comput. Phys. Commun.* **151** 60

[59] Frisch M J, Trucks G W, Schlegel H B, *et al.* 2016 *Gaussian* 16*, Revision C*.01 Gaussian Inc., Wallingford CT

[60] Fonseca Guerra C, Snijders J, Te Velde G T and Baerends E J 1998 *Theor. Chem. Acc.* **99** 391

[61] Parr R G, Ceperley D M and Alder B J 1982 *Phys. Rev. Lett.* **45** 95

[62] Russier V and Badiali J 1989 *Phys. Rev. B* **39** 13193

[63] Brack M 1993 *Rev. Mod. Phys.* **65** 677